IOP Publishing | Astro Ltd Laser Physics Letters
Laser Phys. Lett. **20** (2023) 035204 (6pp) https://doi.org/10.1088/1612-202X/acb43d

Letter

Manipulation of the orbital angular momentum via four-wave mixing in Rb vapor

Ning Liu[1,2], Xuewen Wang[1,2], Jinpeng Yuan[1,2,*], Liantuan Xiao[1,2], Suotang Jia[1,2] and Lirong Wang[1,2,*]

[1] State Key Laboratory of Quantum Optics and Quantum Optics Devices, Institute of Laser Spectroscopy, Shanxi University, 92 Wucheng Road, Taiyuan 030006, People's Republic of China
[2] Collaborative Innovation Center of Extreme Optics, Shanxi University, 92 Wucheng Road, Taiyuan 030006, People's Republic of China

E-mail: yjp@sxu.edu.cn and wlr@sxu.edu.cn

Received 23 December 2022
Accepted for publication 12 January 2023
Published 31 January 2023

Abstract

The manipulation of the orbital angular momentum (OAM) contributes to understand the OAM multiplexing, is significant in free-space optical communication and information processing. We theoretically simulate and experimentally demonstrate the regularity of the OAM transfer, including the angular and radial modes, of Laguerre–Gaussian beam via four-wave mixing process in ^{85}Rb vapor. The 420 nm coherent blue light output field inherits the phase characteristic of 780 nm and 776 nm beams with different OAM modes. The output field OAM modes show the transfer as a typical arithmetic operation of the input field OAM modes with equal-handed angular indice l, while, the conversion between angular and radial modes occurs with the opposite angular indice l. Such rules of the OAM transfer and manipulation have implications on the research of high-capacity information transfer and quantum communication.

Keywords: orbital angular momentum transfer, four-wave mixing, angular and radial indices

(Some figures may appear in colour only in the online journal)

1. Introduction

The orbital angular momentum (OAM) theoretically has an infinite number of eigenstates and is defined in an infinite-dimensional Hilbert vector space [1–4], it has been widely applied in optical communications [5, 6] and remote sensing [7–9]. The OAM of beams provides a fundamentally new freedom degree compared conventional Gaussian beams [4]. Laguerre–Gaussian (LG) beams, as one of the typical OAM beams with two indices including an azimuthal index l related to OAM and a radial index p related to the radial nodes [10, 11]. The manipulation of OAM is significant for comprehending the interplay between radial and azimuthal indices, contributing to further increase the system transmission capacity.

Various nonlinear media provide possible venues for information transmission based on OAM transfer, such as crystals, atomic medium and two-dimensional materials [5, 12, 13]. Within these media, a wide range of nonlinear processes have been extensively investigated to realize the OAM transfer, including sum-frequency generation (SFG), four-wave mixing (FWM), and second-harmonic generation

* Authors to whom any correspondence should be addressed.

(SHG) [14–16]. In particularly, the OAM transfer based on FWM has attracted tremendous attention because the FWM process has strict phase matching conditions, which two (three) frequencies mutually interact to produce two (one) new frequencies, moreover, it prevents any information loss due to linear absorption and permits us to work at high optical depths [17–19].

The atomic medium has emerged as an ideal candidate for OAM transfer owing to the flexible tunability, better beam quality, abundant energy levels [13, 20]. Among previous researches, the transfer about angular index l attracts more attention. The phase information associated with OAM is transferred entirely from the pump light to the blue light in ^{85}Rb vapor by FWM process [21]. The OAM transfer from input optical fields to output optical fields is used to distinguish the two FWM processes in Rb vapor [22]. The OAM transfer between fields involved via a FWM process in Rb vapor for high-efficiency OAM entanglement is quantitatively explored [23]. Recently, the investigation about Gouy phase matching facilitates efficient and controlled angular and radial mode conversion [16]. With only a few studies focusing on radial index p, and there exists no obvious conservation law that led to the conversion between the l and p, the appealing conversion is still required for further deeper and more detailed exploration for the increasement of the bandwidth capacity.

In this work, we theoretically simulate and experimentally demonstrate the regularity for the OAM transfer via FWM in ^{85}Rb vapor. The 420 nm coherent blue light (CBL) output field inherits the phase characteristic when either or both of 780 nm and 776 nm beams with different OAM modes. The OAM modes of the output field show the transfer as an arithmetic operation of the input fields OAM modes with equal-handed angular indice l, while, the esoteric conversion between angular and radial modes occurs with the opposite angular indice l. This study about angular index l and radial index p provides an experimental basis for the high-capacity information transfer, which has the potential to greatly contribute to the development of quantum communication and network.

2. Experiment setup

The relevant energy levels of ^{85}Rb are shown in figure 1(a). When two photons of 780 nm and 776 nm pump the Rb atoms from the $5S_{1/2}$ state to the $5D_{5/2}$ state, a 5233 nm field corresponding to the $5D_{5/2}$–$6P_{3/2}$ transition is produced through ASE process. Then, the 5233 nm optical field combines with the two pump fields, resulting in the 420 nm CBL generation corresponding to the $6P_{3/2}$–$5S_{1/2}$ transition by FWM process. Therefore, the output field inherits the phase information of the input fields because of phase matching.

The experiment setup is shown in figure 1(b). The 780 nm and 776 nm beams are provided by the external cavity diode laser (DL pro, Toptica) and the Ti: sapphire laser system (SolaTis-SRX-XF, M Squared Lasers), respectively. The frequency references of the 780 nm and 776 nm lasers are dependent on the saturation absorption spectrum (SAS) and electromagnetically induced transparency (EIT), respectively. The beams are shaped as LG modes by the vortex retarder. Then, the 780 nm and 776 nm LG beams overlap and propagate in the same direction, and are focused on a 5 cm length Rb vapor cell which is housed in a μ-metal to shield stray magnetic field [24]. Its temperature is accurately controlled by a self-feedback system and maintained at 130 °C, corresponding the atomic density of 3.56×10^{13} cm^{-3}. The CBL output field is separated from the background beam using an interference filter (center wavelength 420 nm, 10 nm pass band) and recorded by a charge-coupled device (CCD) in real time. The tilting lens is used to detect the topological charge numbers of the output field.

3. Results and discussions

The mode-overlap integral of all involved complex electric fields predict the relative probability of generating a particular pair of 420 nm and 5233 nm FWM modes as c, following [16],

$$c = \int_0^{2\pi} \mathrm{d}\theta \int_0^{\infty} r\mathrm{d}r \int_{-L/2}^{L/2} \mathrm{d}z\, u_{780}\, u_{776}\, u_{5233}^{*}\, u_{420}^{*} \tag{1}$$

where the subscripts denote the input electric fields at wavelengths of 780 nm and 776 nm and the generated fields at 5233 nm and 420 nm in figure 1(a). We use cylindrical polar coordinates and assume that the pump fields are focused at the center of the vapor cell with length L.

Any paraxial beams $u\ (r,\ z,\ \theta)$ can be decomposed in the $\mathrm{LG}_p^l(r,\theta,z) = \sqrt{\frac{2p!}{\pi(|l|+p)!}}\ \frac{1}{w(z)}\left(\frac{\sqrt{2}r}{w(z)}\right)^{|l|} e^{-\frac{r^2}{w(z)^2}} \times L_p^{|l|}\left(\frac{2r^2}{w(z)^2}\right) e^{i\Phi_C(z,\,r)}\ e^{i\Phi_G(z)}\, e^{il\theta}$, where $L_p^{|l|}$ is a Laguerre polynomial, p is the radial topological charge and l is the angular topological charge. The beam radius varies with propagation according to $w(z) = w(0)\sqrt{1+z^2/z_{\mathrm{R}}^2}$, and the Gouy phase describes the phase evolution of a mode propagating through a focus, $\Phi_{\mathrm{G}}(z) = -(1+2p+|l|)\arctan\left(\frac{z}{z_{\mathrm{R}}}\right)$, with $z_{\mathrm{R}} = \pi {w_0}^2/\lambda$ denoting the Rayleigh range for a beam waist w_0. Also, $\Phi_C = k\left(z + \frac{r^2}{2}\left(z + z_{\mathrm{R}}^2/z\right)^{-1}\right)$ accounts for wavefront curvature. The azimuthal integral of equation (1) restricts the output modes to those for which the OAM is conserved [16, 21],

$$l_{780} + l_{776} = l_{5233} + l_{420}. \tag{2}$$

The relative Gouy phase between input fields modes $N_p^l = 1 + 2p + |l|$ crucially affects mode conversion. The total mode order must therefore also be conserved, leading to the conservation,

$$\left(N_p^l\right)_{780} + \left(N_p^l\right)_{776} = \left(N_p^l\right)_{5233} + \left(N_p^l\right)_{420}. \tag{3}$$

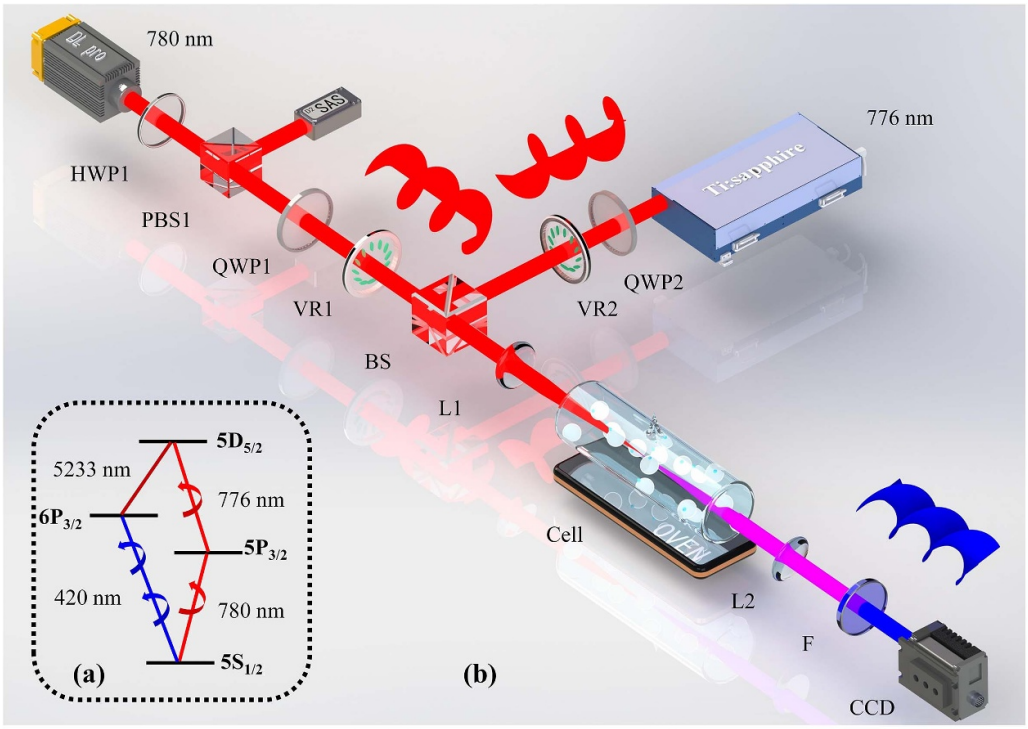

Figure 1. (a) Relevant energy levels of ^{85}Rb. (b) Scheme of the experimental setup. BS, beam splitter; HWP, half-wave plate; M, high-reflection mirror; PBS, polarization beam splitter; QWP, quarter-wave plate; CCD, charge-coupled device; L, lens; F, interference filter; VR, vortex retarder; SAS, saturation absorption spectroscopy.

Here we assume zero order radial modes for the pump lights, then equation (3) can be expressed as [21],

$$|l_{780}| + |l_{776}| = |l_{420}| + |l_{5233}| + 2p_{420} + 2p_{5233}. \quad (4)$$

The 5233 nm infrared beam is currently absorbed by the cell, which is unobserved in the experiment. However, the OAM conservation and Gouy phase matching indicate that it is mainly generated in the fundamental Gaussian mode. In addition, if a sapphire cell is used, the mode of the infrared beam can be directly observed [15, 16, 25].

Figure 2 theoretically simulates the normalized CBL profiles with different modes of 780 nm and 776 nm beams. Both input beams are shaped as LG beams with radial indices $p_{780} = p_{776} = 0$, meanwhile the angular indices $l_{776} = 0, \pm 1, \pm 2$ and $l_{780} = 0, 1, 2$. Two situations discussed here including the two beams OAM modes with equal-handed angular index l and opposite angular index l. Firstly, a simple addition of OAM consists with equation (2) occurs when the two beams with equal-handed angular index l as shown in figures 2(a1)-(a5), (b1)-(b3) and (c1)-(c3). Secondly, the conversion between the angular and radial mode indices that consists with equation (4) occurs with opposite angular index l in figures 2(b4)-(b5) and (c4)-(c5) [23, 26]. With the equal-handed angular index l of input fields, the phase singularity on the beam axis results in a zero axial intensity yielding an annular beam profile. However, when the input fields with opposite l, the CBL profiles display a central vortex surrounded by a number of rings equal $p_{420} + 1$. The radial index p_{420} can be identified from the observed intensity profiles as the number of nodal rings. It can be intuitively seen that $l_{420} = l_{780} + l_{776}$ owing to OAM conservation both in the two situations.

Figures 3(a1)-(a5) show the CBL intensity profiles with $l_{780} = 0, 1, 2, 3, 4$ and $l_{776} = 0$. The powers of the 780 nm and 776 nm lasers are 35 mW and 17 mW, respectively. The laser frequency detunings are adjusted to minimize Kerr lensing, the 780 nm laser is tuned 1.45 GHz blue of the $5S_{1/2}(F = 3)-5P_{3/2}(F = 4)$ transition, while the 776 nm laser resonate with the $5P_{3/2}(F = 4)-5D_{5/2}(F = 5)$ transition [21]. Figure 3(a1) shows the CBL profile with Gaussian distribution [27]. At the same time, the CBL intensity profiles of $l_{420} \neq 0$ in figures 3(a2)-(a5) show a 'donutlike' structure, with a central vortex surrounded by a single ring, also the radius increases with increasement of topological charge l_{420} [21, 28]. In order to detect the topological charge numbers l_{420}, the tilted-lens method is employed and the images are shown in figures 3(b1)-(b5). As for the tilted-lens method, it relies on the fact that a monochromatic optical vortex with topological charge l splits into $|l|$ elementary vortices under astigmatic transformation, revealing $|l|$ tilted dark stripes in its image near the focus [29]. The results not only display a number of dark fringes equal to the value of l_{420}, but also exhibit a 45° rotation corresponds to the sign of the l_{420} [17]. The presented results intuitively obey the transfer of an angular index arithmetic operation $l_{420} = l_{780} + l_{776}$.

A further study of the angular mode indice-l case is investigated here. Figure 4 shows the CBL intensity and tilted-lens detection images with $l_{776} = 0, -1, -2, -3, -4$ and

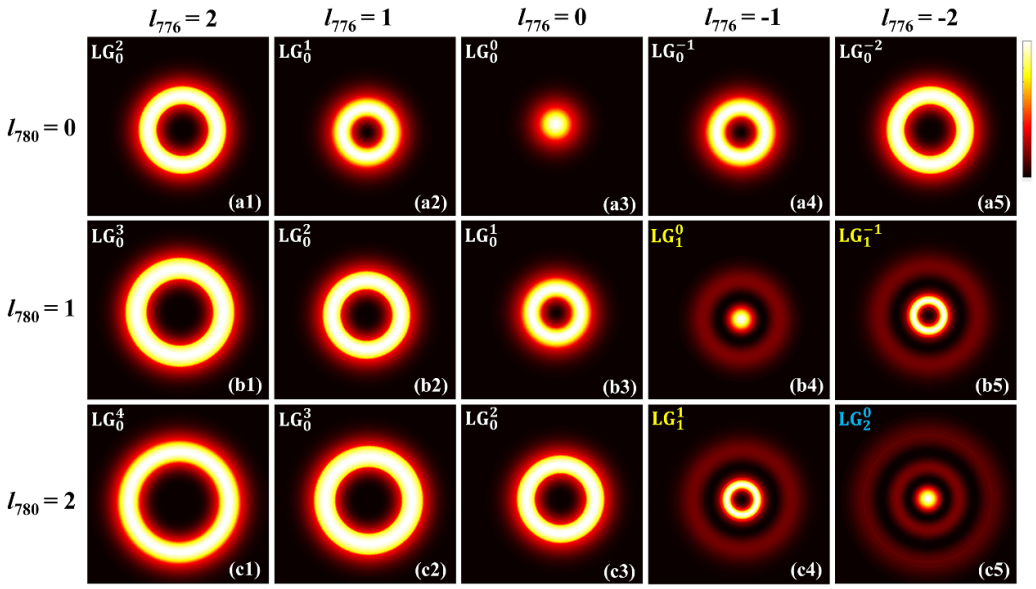

Figure 2. The theoretical CBL profiles arising from mixing 776 nm $LG_0^{0,\pm1,\pm2}$ with 780 nm $LG_0^{0,1,2}$pump modes.

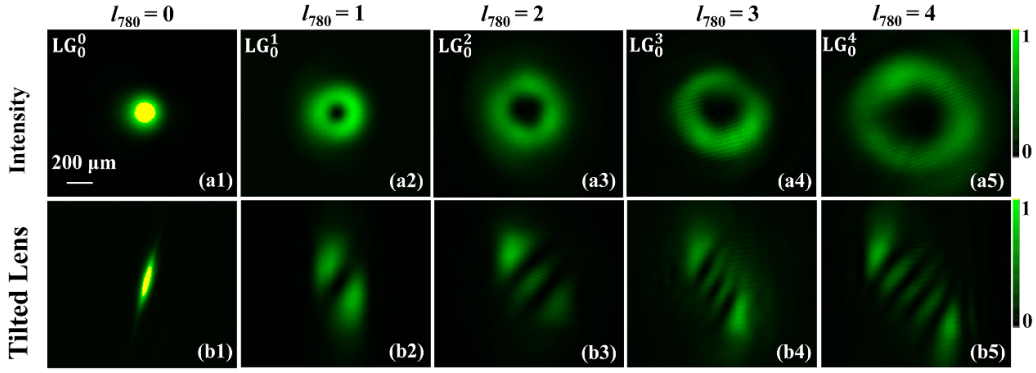

Figure 3. Intensity profiles of CBL (top) and corresponding tilted-lens detection images (bottom) with single-charged vortex beam at 780 nm $LG_0^{0,1,2,3,4}$ and plane wavefront beam at 776 nm LG_0^0 modes.

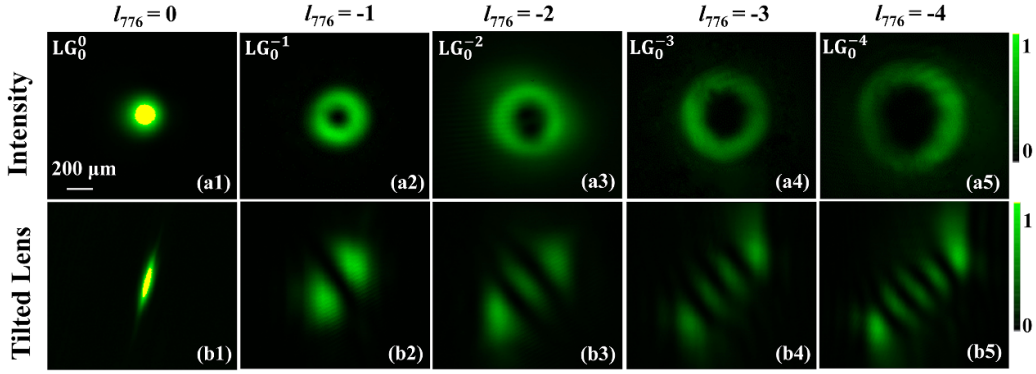

Figure 4. Intensity profiles of CBL (top) and corresponding tilted-lens detection images (bottom) with single-charged vortex beam at 776 nm $LG_0^{0,-1,-2,-3,-4}$ and plane wavefront beam at 780 nm LG_0^0 modes.

$l_{780} = 0$ under the same experimental conditions in figure 3. We observe the 'donutlike' structure, which proves the existence of OAM, meantime, the radius of the ring's scales increasing with the angular index l. The tiled-lens images in figures 4(b1)-(b5) further verify the transfer follows an arithmetic operation and comply with equation (2). Note that,

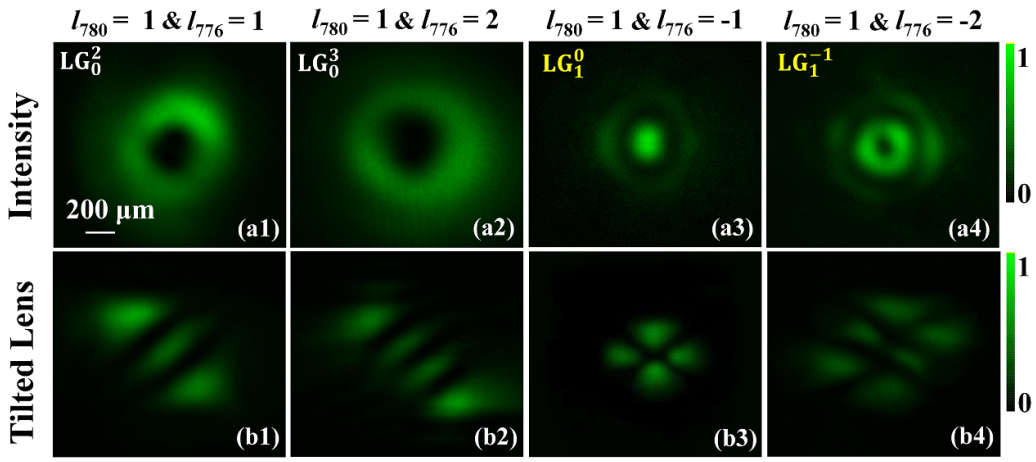

Figure 5. Intensity profiles of CBL (top) and tilted-lens detection images (bottom) arising from mixing 780 nm LG_0^1 with 776 nm $LG_0^{\pm 1,\,\pm 2}$ pump modes.

the dark fringes in figures 3(b1)-(b5) and 4(b1)-(b5) are in opposite directions, as the titled dark fringes whose orientation depends on whether the topological charge is positive or negative.

Figure 5 shows the CBL intensity (top) and corresponding tilted-lens detection images (bottom) when $l_{780} = 1$ and $l_{776} = \pm 1, \pm 2$, and the other conditions are the same as figure 3. Firstly, figures 5(a1)-(a2) show the similar regularity in the cases mentioned above. Secondly, figures 5(a3)-(a4) show the CBL profiles with a central vortex surrounded by a number of rings, which means the existence of radial index when the two beams carry opposite l. Meanwhile, the radius of the central vortex is also changed with the variation of angular index l. Figures 5(b3)-(b4) show the tilted-lens images exhibit orthogonal dark fringes which directly indicate the appearance of radial index p. Also, the tilted-lens detection images exhibit orthogonal dark fringes, where the number of fringes in right and left rotation 45° directions correspond to the values of p and $p + |l|$ [30], respectively. The detection results show that in addition to the OAM conservation $l_{420} = l_{780} + l_{776}$, there is also a conversion between the angular and radial modes coinciding with equation (4).

4. Conclusion

In summary, we theoretically simulate and experimentally demonstrate transverse intensity profiles of the generated CBL when 780 nm and 776 nm beams carrying equal-handed and opposite angular indices l via FWM process in ^{85}Rb atoms. The results prove that the OAM transfer obey an arithmetic operation of the input fields with equal-handed angular index l. Also, the conversion between angular and radial modes occurs when the input fields with opposite angular index l due to the Gouy phase. Such a complete comprehension about the radial index p has the possibility to convert efficiently between radial and azimuthal modes, allowing access to the full state space for spatial mode encoding, with potential applications in all-optical communications.

Acknowledgments

This work is supported by the NSFC under Grant Nos. 61875112, 62075121; Program of Graduate Education and Teaching Reform in Shanxi Province Grant No. 2022YJJG012; and the Fund for Shanxi '1331 Project'.

References

[1] Meng F, Wei X, Qu Y, Chen Y, Zhang X, Kang Z, Wang L, Wang H and Gao J 2022 *J. Lumin.* **242** 118551
[2] Fickler R, Lapkiewicz R, Plick W N, Krenn M, Schaeff C, Ramelow S and Zeilinger A 2012 *Science* **338** 640–3
[3] Kovalev A A and Kotlyar V V 2021 *Optik* **242** 166863
[4] Wang J *et al* 2012 *Nat. Photon.* **6** 488–96
[5] Qiu Z, Cao B, Huang K, Zhang X and Lu X 2022 *Optik* **258** 168828
[6] Lopez R P, Ruiz U, Arrizon V and Garcia R R 2016 *Opt. Lett.* **41** 4138–41
[7] Tao S H, Yuan X C, Lin J, Peng X and Niu H B 2005 *Opt. Express* **13** 7726–31
[8] Lavery M P J, Barnett S M, Speirits F C and Padgett M J 2014 *Optica* **1** 1–4
[9] Götte J B, O'Holleran K, Preece D, Flossmann F, Arnold S F, Barnett S M and Padgett M J 2012 *Science* **338** 640–3
[10] Yao A M and Padgett M J 2008 *Opt. Express* **16** 993–1006
[11] Trichili A, Guzman C R, Dudley A, Ndagano B, Salem A B, Zghal M and Forbes A 2016 *Sci. Rep.* **6** 27674
[12] Asadpour S H, Paspalakis E and Hamedi H R 2021 *Phys. Rev.* A **103** 063705
[13] Wang S, Yuan J, Wang L, Xiao L and Jia S 2019 *Laser Phys. Lett.* **16** 125204
[14] Chopinaud A, Jacquey M, Viaris de Lesegno B and Pruvost L 2018 *Phys. Rev.* A **97** 063806
[15] Ge Z, Yang C, Li Y, Li Y, Liu S, Niu S, Zhou Z and Shi B 2022 *Chin. Phys.* B **31** 104210
[16] Offer R F, Daffurn A, Riis E, Griffin P F, Arnold A S and Franke Arnold S 2021 *Phys. Rev.* A **103** L021502
[17] Kong F *et al* 2017 *Nat. Commun.* **8** 14970
[18] Gariepy G, Leach J, Kim K T, Hammond T J, Frumker E, Boyd R W and Corkum P B 2014 *Phys. Rev. Lett.* **113** 153901

[19] Verma O N, Pandey R K, Yadav R R and Patel A 2022 *Phys. Rev.* A **106** 053713
[20] Wang X, Yuan J, Wang L, Xiao L and Jia S 2022 *Opt. Laser Technol.* **149** 107874
[21] Walker G, Arnold A S and Franke Arnold S 2012 *Phys. Rev. Lett.* **108** 243601
[22] Akulshin A M, McLean R J, Mikhailov E E and Novikova I 2015 *Opt. Lett.* **40** 1109–12
[23] Offer R F, Stulga D, Riis E, Franke Arnold S and Arnold A S 2018 *Commun. Phys.* **1** 84
[24] Wang S, Yuan J, Wang L, Xiao L and Jia S 2021 *Front. Phys.* **16** 12502
[25] Paterson L, MacDonald M P, Arlt J, Sibbett W, Bryant P and Dholakia K 2001 *Science* **292** 912–4
[26] Yuan J, Liu H, Wang L, Xiao L and Jia S 2021 *Opt. Express* **29** 4858–65
[27] Vernier A, Arnold S F, Riis E and Arnold A S 2010 *Opt. Express* **18** 17020–6
[28] Yuan J, Wu C, Li Y, Wang L, Zhang Y, Xiao L and Jia S 2019 *Opt. Express* **27** 92–101
[29] Denisenko V, Shvedov V, Desyatnikov A S, Neshev D N, Krolikowski W, Volyar A, Soskin M and Kivshar Y S 2009 *Opt. Express* **17** 23374–9
[30] Downes L A, Whiting D J, Adams C S and Weatherill K J 2022 *Opt. Lett.* **47** 6001–4